Gas permeability evolution of cataclasite and fault gouge in triaxial compression and implications for changes in fault-zone permeability structure through the earthquake cycle

Shin-ichi Uehara[a,*], Toshihiko Shimamoto[b]

[a] Institute of Petroleum Engineering, Heriot-Watt University, Edinburgh, EH14 4AS, UK
[b] Department of Geology and Mineralogy, Graduate School of Science, Kyoto University, Kyoto 606-8502, Japan

Abstract

We report the results of permeability measurements of fault gouge and tonalitic cataclasite from the fault zone of the Median Tectonic Line, Ohshika, central Japan, carried out during triaxial compression tests. The experiments revealed marked effects of deformation on the permeability of the specimens. Permeability of fault gouge decreases rapidly by about two orders of magnitude during initial loading and continues to decrease slowly during further inelastic deformation. The drop in permeability during initial loading is much smaller for cataclasite than for gouge, followed by abrupt increase upon failure, and the overall change in permeability correlates well with change in volumetric strain, i.e., initial, nearly elastic contraction followed by dilatancy upon the initiation of inelastic deformation towards specimen failure. If cemented cataclasite suffers deformation prior to or during an earthquake, a cataclasite zone may change into a conduit for fluid flow. Fault gouge zones, however, are unlikely to switch to very permeable zones upon the initiation of fault slip. Thus, overall permeability structure of a fault may change abruptly prior to or during earthquakes and during the interseismic period. Fault gouge and cataclasite have internal angles of friction of about 36° and 45°, respectively, as is typical for brittle rocks.
© 2003 Elsevier B.V. All rights reserved.

Keywords: Fluid flow; Permeability; Triaxial deformation; Median Tectonic Line; Fault gouge; Cataclasite; Earthquake

1. Introduction

Fault zones may act as barriers, conduits, or mixed conduit/barrier systems, which form important components of fluid flow regimes operating in the crust (e.g. Caine et al., 1996). To estimate the permeability structure of fault zones, several studies have reported the permeability measurements of natural fault rocks. Evans et al. (1997) divided the fault zone of the East Fork thrust faults in the Washakie Range, Wyoming, USA into fault core, damage zone and protolith, and they report permeability values of representative samples from each zones. They clearly elucidated a now widely accepted permeability structure of fault zones consisting of a low-permeability fault core and permeable damage zone. Seront et al. (1998) collected

* Corresponding author. Fax: +44-131-451-3127.
E-mail addresses: shin.uehara@pet.hw.ac.uk (S. Uehara),
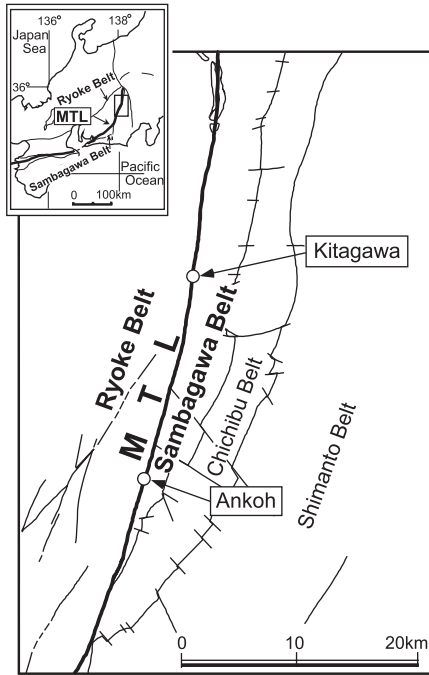shima@kueps.kyoto-u.ac.jp (T. Shimamoto).

Fig. 1. Location of the sampling area and regional setting of the Median Tectonic Line and metamorphic belts in central Japan.

samples from the Stillwater fault zone, a normal fault in central Nevada, USA and measured the permeability of fault rocks under hydrostatic pressures. They also measured differential stress and pore volume strain under triaxial compression, although they did not measure the evolution of permeability with deformation. From the results of permeability and differential stress measurements, they discussed fault mechanics prior to catastrophic rupture while considering fluid flow and pore pressure evolution in the core zone. Wibberley and Shimamoto (2003) investigated internal structure and permeability of the fault zone of the Median Tectonic Line (MTL; the largest strike-slip fault in Japan) in western Mie Prefecture, S.W. Japan and found complex permeability structures reflecting the long tectonic history of this fault. They also showed that the core of this fault zone, consisting of a continuous and very planer clayey fault-gouge zone, is very impermeable and thermal pressurization is likely during seismic slip here. However, all these previous studies only measured permeability under hydrostatic pressure, although permeability changes during deformation

need to be known to analyze fluid flow in fault zones associated with earthquakes.

Investigating the permeability evolution of fault rocks during deformation is thus important because fault zones are subject to intense shearing deformation prior to, during and even after earthquakes and because the fault zone may heal during the interseismic period causing long-term permeability reduction. Previous work on permeability changes during deformation of rocks and incohesive materials suggests that effects of deformation on the permeability of fault rocks depend on the type of fault rocks (e.g. Zoback and Byerlee, 1975; Morrow et al., 1984; Zhu and Wong, 1997, 1999; Zhang and Tullis, 1998; Zhang and Cox, 2000). However, only a few studies report permeability evolutions of fault rocks during deformation (Lockner et al., 2000). We thus report herein our measurements of permeability changes during triaxial deformation of fault gouge and tonalitic cataclasite collected from the Median Tectonic Line in Ohshika, central Japan. Studies of mylonites in Japan were first carried out here and this area is one of the classical, best studied areas of the MTL fault zone. We then discuss possible changes in
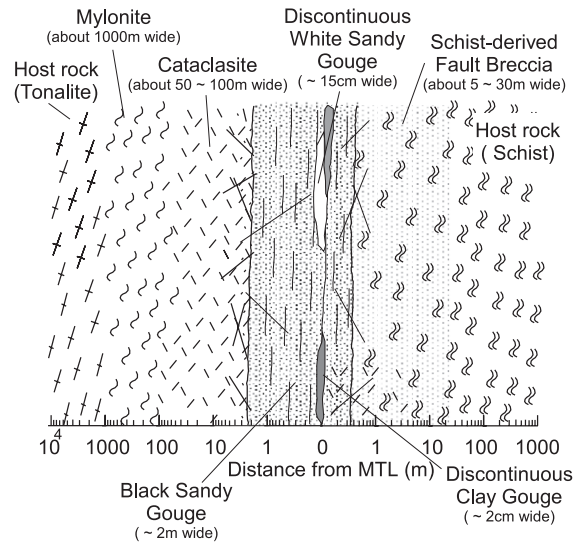

Fig. 2. A schematic sketch showing internal structure of the MTL fault zone at Ohshika mura, central Japan, based on the field work of Uehara (2002). Horizontal scale indicates typical widths of representative fault rocks.

Table 1
Specimens and conditions for experiments

Sample	Locality	P_c [MPa]	P_p [MPa]	Length [mm]	Diameter [mm]	Axial displacement rate [mm/s]	Comments
Cataclasite							
AK0916A	Ankoh	30.2	20	43.8	20.5	0.001	Strain gauge used
AK0916A	Ankoh	39.5	20	41.3	20.4	0.0005	
AK0916A	Ankoh	71	20	40	20.2	0.0001	
AK0916C	Ankoh	40.2	20	24.2	20.4	0.001	
AK0916C	Ankoh	71.5	20	22.4	20.5	0.001	
AK0916C	Ankoh	98.5	20	24.9	20.6	0.001	
Fault gouge							
KG1203B	Kitagawa	20.3	0−0.6	43.5	24.1	0.001	
AK02A8	Ankoh	49.8	0−0.74	37.3	24.3	0.001	
KG1102	Kitagawa	80.7	0−0.62	37.2	24.4	0.001	

'Ankoh' and 'Kitagawa' at 'Locality' are the name of the MTL outcrops at Ohshika (Uehara, 2002).

'P_p' and 'P_c' are pore pressure and confining pressure, respectively.

The value at 'P_p' of fault gouge shows pore pressure at downstream and that at upstream; for example, '0−0.6' means that pore pressure is 0 MPa at downstream and 0.6 MPa at upstream.
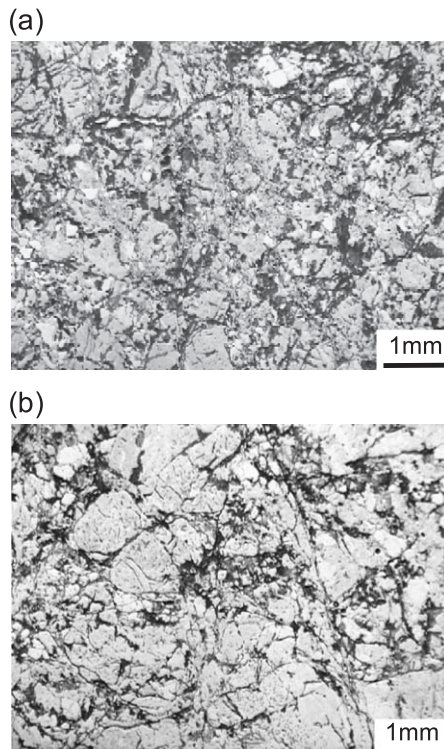

Fig. 3. Photomicrographs of cataclasite, (a) AK0916A and (b) AK0916C, under plane-polarized light.

permeability structure of a fault zone during earthquake cycles.

2. Internal structure of the MTL fault zone around Ohshika and sample description

The MTL is the largest strike slip fault in Japan extending over 1000 km from Kyushu to Kanto districts and it bounds two contrasting metamorphic belts, the Ryoke belt of the low P/high T type and the Sambagawa belt of high P/low T type (Fig. 1). The MTL fault zone consists of a range of fault rocks, i.e., incohesive fault rocks along the MTL, cataclasites, and mylonites on the Ryoke side, reflecting its long tectonic history (Hara et al., 1977, 1980; Takagi, 1983, 1984, 1986; Michibayashi and Masuda, 1993; Michibayashi, 1993; Matsushima, 1994; Tanaka et al., 1996).

We used cataclasite and fault gouge collected from the MTL fault zone at Ohshika-mura, Kami-ina-gun, Nagano Prefecture, central Japan (simply called "Ohshika" hereafter; Fig. 1), to study the effect of deformation on fault-rock permeability. Uehara (2002) reports internal structures of the MTL fault zone at Ohshika across the Kitagawa and Ankoh outcrops and
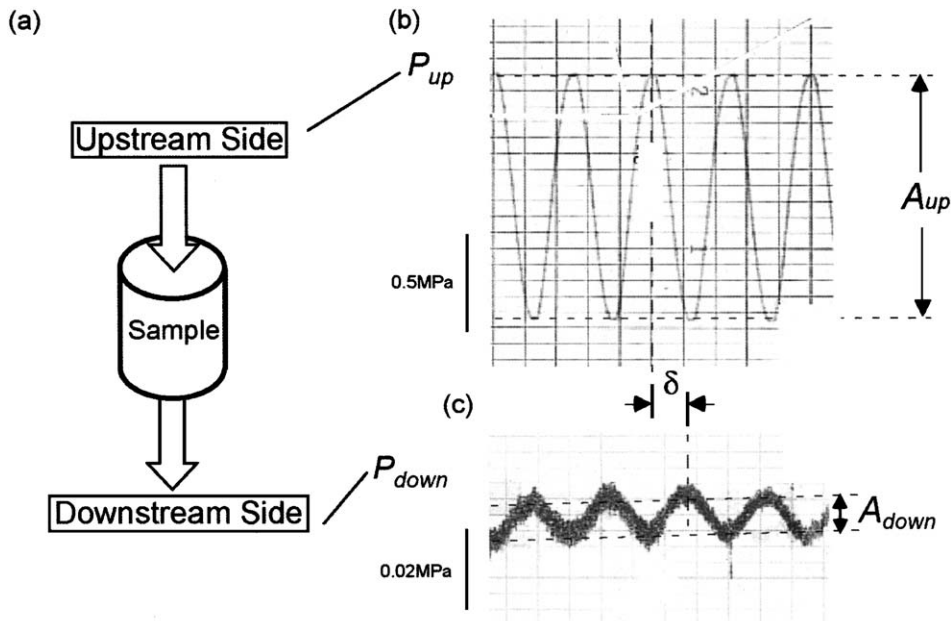
Fig. 4. An example of oscillated upstream pore pressure (upper-right diagram) and subsequent oscillation in the downstream pore pressure (lower-right diagram) for permeability measurement with the pore pressure oscillation method, as recorded on a strip-chart recorder (run number: AK0916A, $P_e = 19.5$ MPa).

their vicinities. The fault zone itself is variable from place to place, but overall it comprises mylonites (about 1000 m wide), cataclasites (about 50–200 m wide) and incohesive fault rocks (about 5–30 m wide) as schematically shown in Fig. 2. The fault core consists of a black sandy gouge zone up to about 2 m in width and discontinuous clayey gouge of 10 to 20 mm in thickness. The schist-derived fault breccia, up to about a few tens of meters wide, is developed and no mylonite zones have been found on the Sambagawa

side. Cataclasite samples used in our experiments were collected from the cataclasite zone on the Ryoke side, less than 3 m away from the boundary between the cataclasite zone and fault gouge zone. This cataclasite is derived mainly from tonalitic mylonites, and it is partially brecciated by later deformation and is cemented with carbonates and some colored minerals. We also used black sandy gouge collected from the MTL fault core. This gouge consists of quartz, carbonate, mica minerals and other clay minerals (smectite, kaolinate), as also found by Tanaka et al. (1996). Here, "sandy" means that this fault gouge is coarse in comparison to clayey gouge, and has a typical grain size of 0.1–0.25 mm. Thin section observation reveals heterogeneity of this gouge in the clast content and in matrix microstructures.

3. Sample preparation and experimental conditions

Two samples of Ryoke cataclasite, AK0916A and AK0916C, were cored in the laboratory and were

Table 2
Range of frequency of oscillation and minimum amplitude ratio

Sample	P_e [MPa]	Frequency of oscillation [Hz]		Minimum amplitude ratio (A_{down}/A_{up})	Phase lag (δ: deg.)
		Before rupture	After rupture		
AK0916A	10.2	0.025	0.25	0.0028	89.6–101
	19.5	0.005,0.01	0.05	0.0015	88.9–139
	51	0.001	0.002	0.00034	89.9–188
AK0916C	20.2	0.25	0.5,1,2	0.0037	88–122
	51.5	0.025	0.1,0.15	0.0052	119–158
	78.5	0.005,0.01	0.1,0.2	0.0013	88–167

surface-ground to make specimens of 20 mm in diameter and 22 to 45 mm in length (Table 1). Although the two samples are quite similar to the naked eye, thin section observation showed that AKO916A has a higher proportion of fine grained material than AK0916C (Fig. 3). Although it is desirable to make specimen length about 2.5 times larger than its diameter (e.g. Paterson, 1978), we could not drill the AK0916C sample long enough to make such specimens due to the presence of fractures. Fault gouge samples were collected by pushing a stainless steel tube of 25-mm inner diameter into the outcrop, and they were squeezed into polyolefin jackets for experimentation. Most gouge samples were cored parallel to their foliation and/or MTL central fault core zone, but a few samples were collected perpendicular to it.

In order to eliminate any pore water, specimens were dried at a temperature of 80 °C for several days prior to permeability measurements. Then specimens were set in the pressure vessel. We used the gas-medium triaxial apparatus at Kyoto University (see Wibberley and Shimamoto, 2003) for deformation and fluid-flow experiments at room temperature and at effective pressures to 80 MPa, using nitrogen as both pore fluid and confining medium (see Table 1 for experimental conditions). "Effective pressure" is defined herein as the difference between confining pressure and pore pressure.

The permeability of cataclasite was measured using the oscillation method developed by Kranz et al. (1990) and Fischer and Paterson (1992), in which pore pressure in the upstream reservoir is oscillated sinusoidally and pore pressure in the downstream reservoir is measured. Permeability and storage capacity can be estimated from the amplitude ratio and the phase shift of the pore pressure in the two reservoirs (see an example of our record in Fig. 4). The storage capacity could not be measured accurately in our experiments because the downstream reservoir volume was not small enough for consistent results at different oscillation frequencies. The average pore pressure in the upstream reservoir was 20 MPa, and its amplitude was set at around 2 MPa in all measurements. The frequencies, minimum value of the amplitude ratio of pore pressure oscillation at downstream reservoir to that at upstream reservoir and the phase lag are given in Table 2. The

permeability of black gouge was measured using a simple gas-flow method under a constant pressure difference across the specimen. The downstream side of specimen was open to atmosphere and the upstream pore pressure during the flow tests is given in Table 1.

The axial displacement rate was 0.001 mm/s except for two runs of AK0916A (Table 1). Effective pressure P_e was around 20, 50, and 80 MPa for AK0916C and black gouge specimens, and it was around 10, 20, and 50 MPa for AK0916A specimens (Table 1). The axial displacement and the axial load were measured outside the pressure vessel. Axial and circumferential strains during deformation of a specimen from sample AK0916A were measured with two strain gauges bonded directly to the specimen with Cyanobond RP-QS, one parallel to the specimen axis and the other in the circumferential direction (Fig. 5). An electrical wire going through a hole in the polyolefin jacket was sealed with epoxy to prevent gas leak from the confining medium to the pore pressure system.
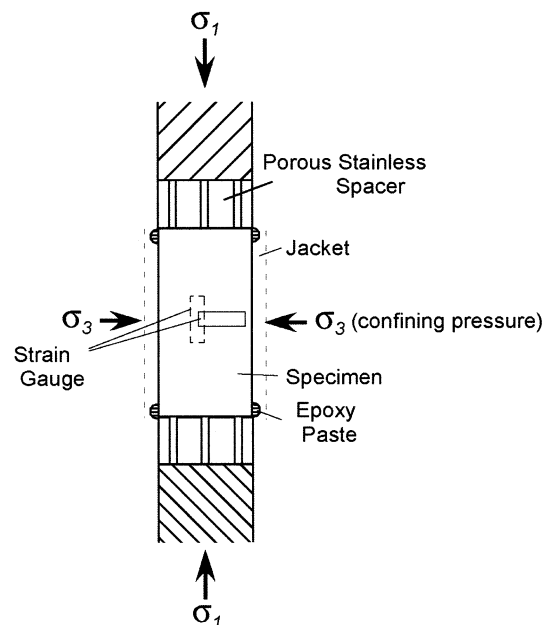

Fig. 5. Specimen assembly for deformation and permeability experiment on cataclasite sample AK0916A. Strain gauges bonded directly on the sample and epoxy paste were not put on the other samples.

Epoxy paste was put on the specimen edges for this specimen to minimize the effect of stress concentrations (Mogi, 1967). However, the effect of this epoxy might not have been enough in our tests, since a fracture developed at the edge. Using specimens shorter than an ideal length could have fostered these end effects. Thus, our experiments are not of high quality in terms of strength measurements of cataclasite.

4. Experimental results

Permeability measurements of MTL fault rocks at effective pressures to 180 MPa by Uehara (2002) determined the overall permeability structure of the MTL at Ohshika. Fig. 6 shows his results at $P_e = 80$ MPa using the same horizontal axis for the MTL

internal structure in Fig. 2. Ryoke mylonite and cataclasite, and Ryoke and Sambagawa metamorphic rocks have permeability below 10^{-18} m^2, whereas the permeability of incohesive fault gouge is greater by more than two orders of magnitude. Clayey fault gouge exhibits intermediate permeability values. Thus, the incohesive fault zone constitutes a permeable zone for fluid flow. A very impermeable and pervasive fault-gouge zone, such as the one recognized by Evans et al. (1997) and by Lockner et al. (2000), is missing at Kitagawa and Ankoh outcrops of MTL at Ohshika. This may be due to discontinuous clayey fault gouge in Ohshika which might have been distorted by the latest movement on the MTL. Locations and permeability of the samples used in the deformation and fluid-flow experiments described in this paper are shown with open circles in Fig. 6 (cf. Table 1).
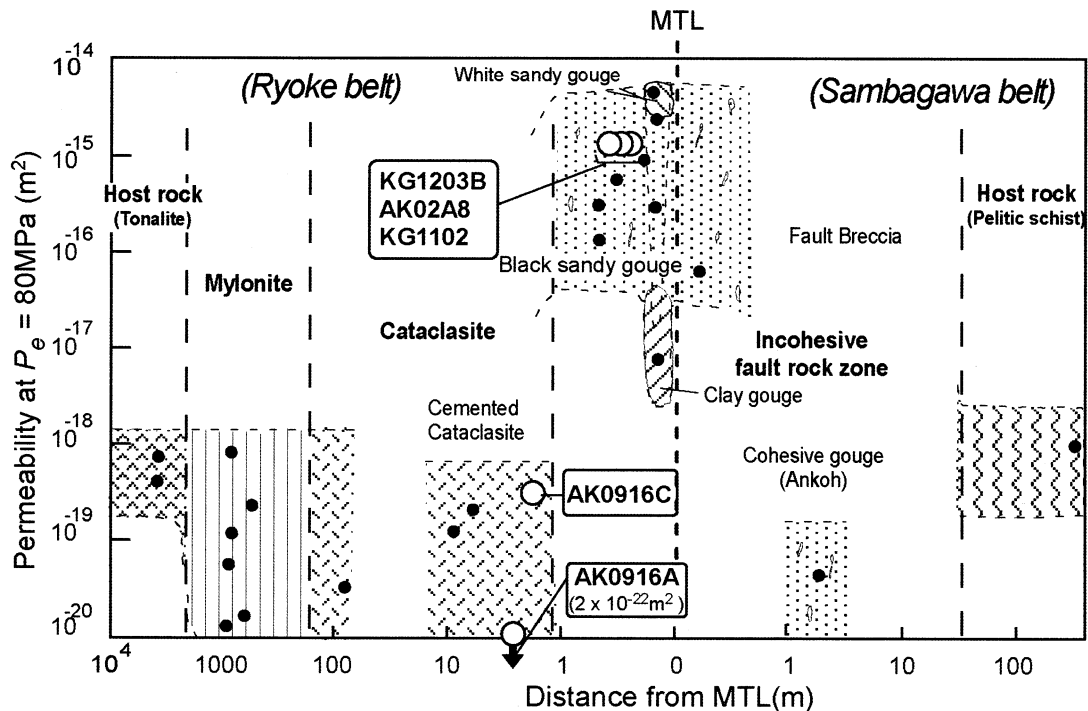

Fig. 6. Permeability structure of the MTL fault zone as indicated by measured values (filled circles) of nitrogen gas permeability at an effective, hydrostatic pressure P_e of 80 MPa. The horizontal scale of this figure corresponds to the structure of the MTL fault zone in Fig. 2. Open circles show locations and permeability values of the samples. Permeability values of samples AK0916A, KG1203B and AK02A8 at $P_e = 80$ MPa were not measured. Those of KG1203B and AK02A8 were estimated from the measured values of nearby samples. The permeability value of AK0916A was estimated from the exponential function fitting well the permeability values of the same sample at $P_e = 10.2$, 19.5 and 51 MPa.
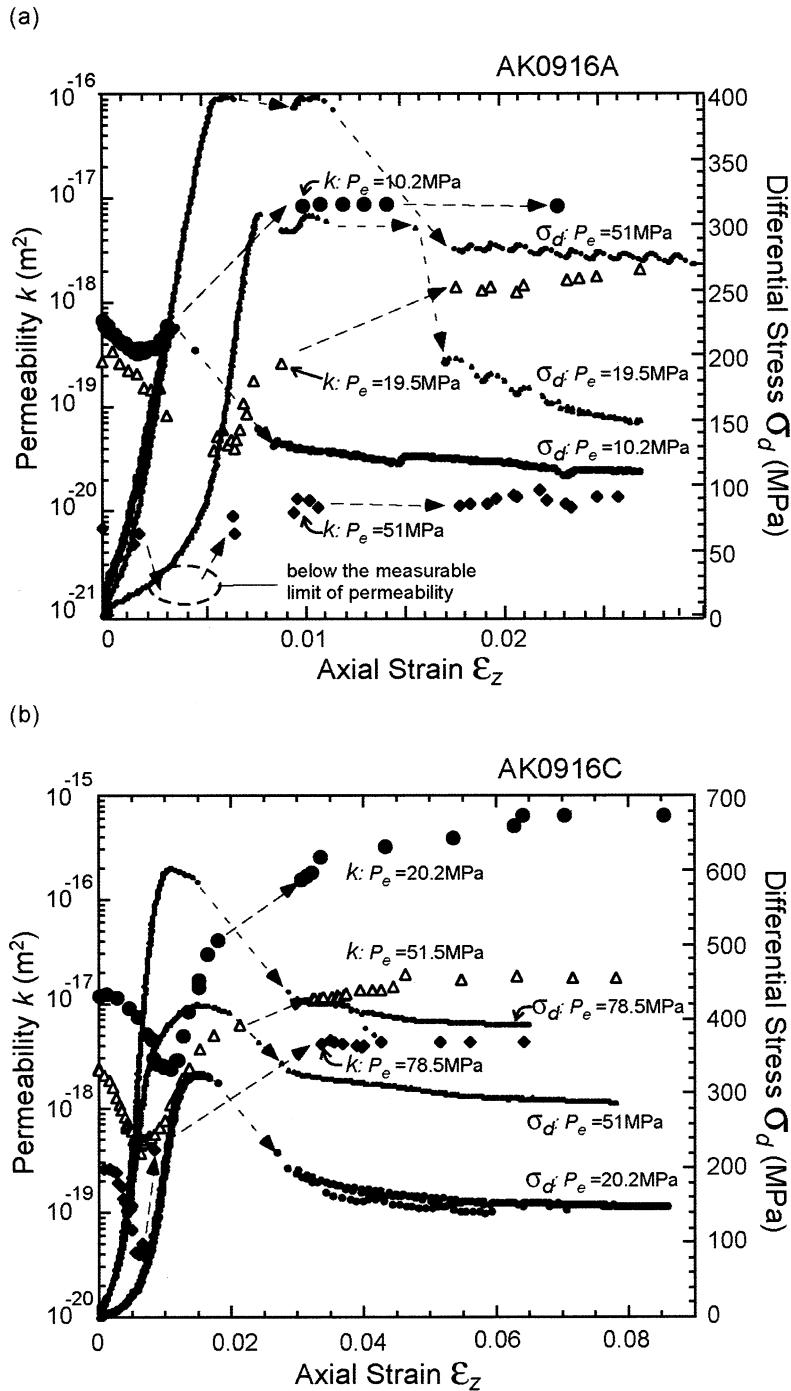
(a)

(b)

Fig. 7. Permeability and differential stress of specimens from (a) AK0916A and (b) AK0916C as functions of the axial strain. P_e is the effective pressure and is given on top of each diagram. The lack of permeability data in the encircled portion with dashed line in (a) for the case of $P_e = 51$ MPa is due to the low permeability below the measurable limit.

4.1. Permeability evolution of cataclasite in triaxial compression

Fig. 7 shows the differential stress and permeability changes during triaxial compression tests at various confining pressures. Externally measured axial displacement was corrected for apparatus distortion to determine the axial strain on the horizontal axis. Differential stress versus axial strain curves all display initial nonlinear portions, nearly linear portions, nonlinear portions prior to the failure points, stress drops and gradual loss of strength towards residual strength. All six specimens have greater ultimate strength at higher effective pressures (see six curves in Fig. 7). The initial nonlinear portion is large for one specimen deformed at $P_e = 19.5$ MPa in (a) and one specimen deformed at $P_e = 20.2$ MPa in (b). Sample AK0916A, fractured more than sample AK0916C, exhibits more complex post-failure behaviors (Fig. 7a). However, in all runs for AK0916C (Fig. 7b), the failure point or peak strength was followed by a gradual drop in strength, then specimen failure accompanied by a stress drop (shown as dashed lines), and finally a slower reduction in strength with further deformation.

Although the overall level of permeability is greater for sample AK0916C (Fig. 7b) than for AK0916A (Fig. 7a), permeability changes with deformation in more or less similar manners in all six cases. Permeability decreases initially down to $0.1-0.2$ of its initial value when the differential stress reaches around $0.3-0.4$ of the failure strength (or the maximum differential stress), then turning to increase and become $30-200$ times as large as its initial value when the stress reaches around $0.7-0.95$ of the failure strength. In a run at $P_e = 51$ MPa in Fig. 7a, the minimum permeability could not be measured because it was below the measurable limit of permeability (somewhat larger than 10^{-21} m^2). Permeability increases abruptly by up to 1.5 orders of magnitude upon failure and continues to increase slowly with further deformation. An exception to this is the run at $P_e = 51$ MPa in which permeability stayed nearly the same after the failure strength was exceeded.

Fig. 8 shows permeability changes against axial strain, ε_z, circumferential strain ε_θ, and volumetric strain, ε_v, prior to the failure point. Permeability clearly changes with volumetric strain; it decreases as the specimen contracts initially and turns to increase with the onset of dilatancy prior to the failure.

4.2. Permeability evolution of fault gouge in triaxial compression

The evolution of the permeability of black gouge during triaxial deformation (Fig. 9) is totally different from those of cataclasite, although a major fault, or a narrow shear zone also formed in the gouge samples. The differential stress versus axial strain curves are characterized by much smaller initial slopes than those for cataclasite (cf. Figs. 7
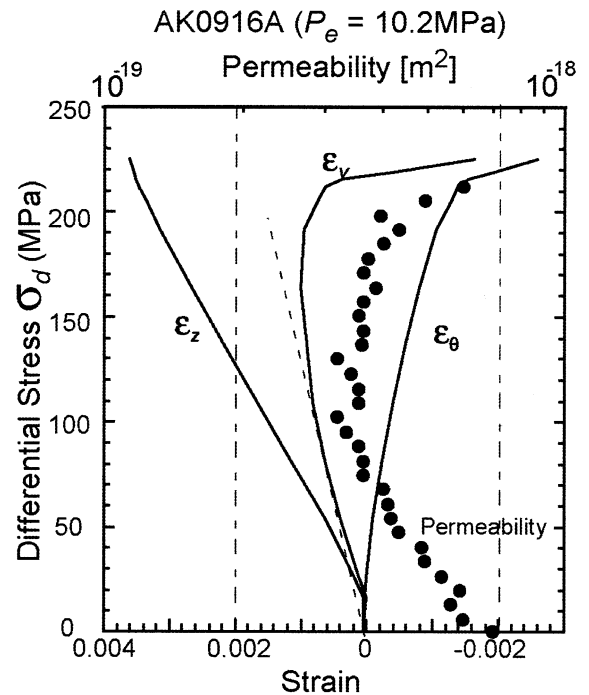

Fig. 8. Permeability and strains of the specimen from AK0916A as functions of the differential stress when effective pressure is 10.2 MPa. The axial and circumferential strains were measured by strain gauges, and the volumetric strain was calculated from them. ε_z, ε_θ and ε_v are the axial strain, the circumferential strain and the volumetric strain respectively. Dotted vertical lines show the measurement limit of the strain gauges, although the strain gauge output monitoring was continued beyond these limits.
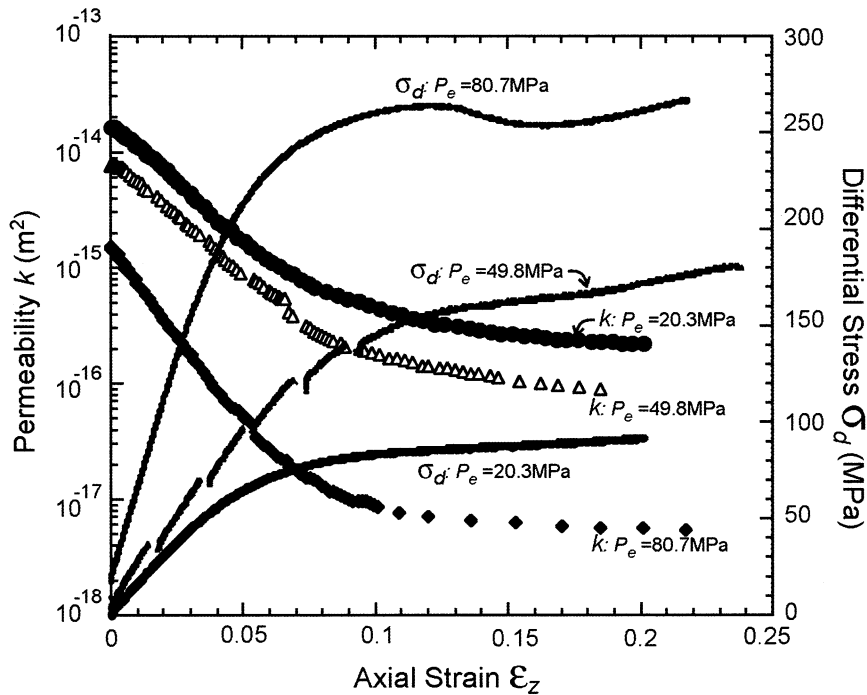
Fig. 9. Permeability and differential stress of specimens from black sandy gouge as functions of the axial strain. P_e is effective pressure. Small steps on the differential stress versus axial strain curve at $P_e = 49.8$ MPa are due to pauses of loading for about 1 min to read strain gauge outputs (not reported here).

and 9), the initial slope being notably greater at lower effective pressures. Permeability drops about two orders of magnitude during this initial loading. At $P_e = 80.7$ MPa, the stress–strain curve shows a broad peak strength followed by slight drop and subsequent slow increase in the differential stress with further deformation. On the other hand, the differential stress continues to increase slowly with deformation at $P_e = 49.8$ MPa and it stays at the same level at $P_e = 20.3$ MPa. Permeability continues to decrease slowly with deformation during this post-yielding behaviors.

It must be noted, however, that differential stress in Fig. 9 was not corrected for the change in the cross-sectional area of the specimen because strain gauges could not be bonded on gouge specimens and the circumferential strain was not measured for the runs. This area correction is larger for Fig. 9 than for Fig. 7 since the axial strain is larger in Fig. 9. With this area correction, the stress–strain

curves, at least those at $P_e = 80.7$ and 20.3 MPa, will exhibit broad strength peaks.

4.3. Strength of cataclasite and gouge

Both cataclasite samples have about the same strength (Fig. 7) and their ultimate strength (a point of maximum differential stress) is plotted as Mohr circles in Fig. 10a. A linear Mohr envelope fits the data reasonably well, giving Coulomb's failure criterion of $\tau = 38$ MPa $+ 1.01\sigma_e$ where τ and σ_e are the shear stress and the effective normal stress on the most favorable failure plane, respectively. This criterion corresponds to the internal angle of friction of $45°$, as is typical of brittle rocks. The ultimate strength is not clearly recognized for gouge (Fig. 9) so that we conventionally defined "yield point" as the point of maximum curvature or the point where the stress–strain curve is bent most sharply to quantify the gouge strength. Morh circle presen-

(a)

Cataclasite

$\tau = 38\text{MPa} + 1.01\sigma_e$

45deg

τ (MPa)

300

100

0   100   500

σ_e (MPa)

(b)

Black Sandy Gouge

$\tau = 4.9\text{MPa} + 0.75\sigma_e$

36deg

τ (MPa)
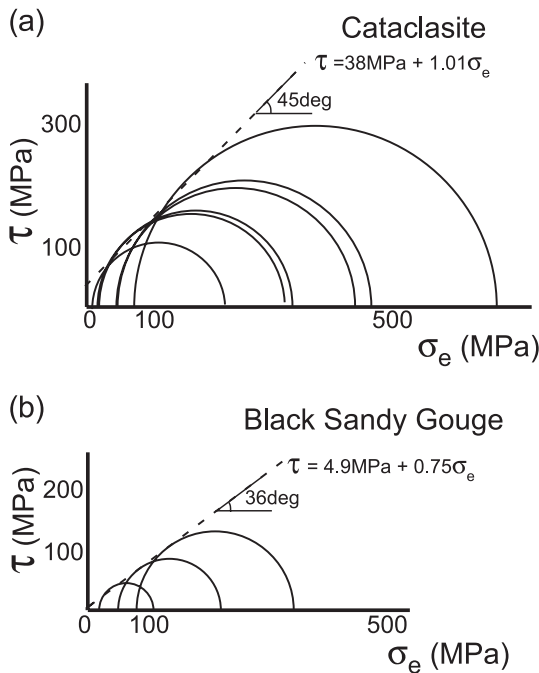
200

100

0   100   500

σ_e (MPa)

Fig. 10. Mohr envelopes (a) for the ultimate strength or the maximum differential stress of cataclasite samples AK0916A and AK0916C and (b) for the yield strength of black sandy gouge (cf. stress–strain curves in Figs. 7 and 9).

tation in Fig. 10b gives Coulomb's yield criterion of $\tau = 49$ MPa $+ 0.75\sigma_e$ with the angle of internal friction of $37°$.

5. Discussion

Permeability changes of cataclasite with deformation shown in Figs. 7 and 8 are typical of brittle rocks and are similar to those reported previously for Westerly granite by Zoback and Byerlee (1975). Crack closure upon the initiation of loading (cf. Walsh, 1965) and volume reduction during nearly elastic deformation in triaxial compression apparently caused the initial reduction in permeability. The variation in the initial nonlinear portion of the stress–strain curve in Fig. 7 is probably due to the variation in the pre-existing fractures in cataclasite samples. Good correlation between permeability and volumetric strain in Fig. 8 indicates that the increase in permeability from slightly below the midway to the failure point is

caused by the dilatancy of the specimen owing to the creation of new microcracks and to the growth of existing microcracks (cf. Brace et al., 1966). Formation of macroscopic fractures in the specimen is no doubt responsible for the sudden and large increase in permeability upon specimen failure (Fig. 7).

The permeability of cataclasite sample AK0916C is greater than that of sample AK0916A by nearly three orders of magnitude (cf. Fig. 7a and b) despite the fact that the latter is fractured into finer fragments than the former (Fig. 3). This suggests that fluid flow along thorough-going fractures is more effective than through fragmented portions.

Deformation behavior and permeability change of black sandy gouge during initial loading are totally different from that of cataclasite (Fig. 9). The slopes of the nearly linear portions of the differential stress versus axial strain curves for cataclasites are about the same for results at different effective pressures (Fig. 7). For the gouge, however, the initial slope notably increases with increasing effective pressure (Fig. 9), suggesting that larger compaction under higher effective pressure suppresses further compaction during the loading in triaxial compression. Unlike the complex change in permeability for cataclasite, the black sandy gouge exhibits continued reduction in permeability with deformation, indicating that compaction occurs throughout the deformation. Compaction is reduced, but must be still taking place even after the yielding of gouge because permeability continues to decrease slowly. Similar change in permeability with deformation has been recognized for fault gouge (Morrow et al., 1984; Lockner et al., 2000; Zhang and Cox, 2000) and for sandstones (Zhu and Wong, 1997).

The results in Figs. 7–9 suggest that the permeability structure of a fault zone may change with time during an earthquake cycle as shown in Fig. 11. Initially, the cohesive cataclasite zone comprises an impermeable zone and the incohesive fault zone constitutes a conduit for fluid flow (left portion of Fig. 11). With stress building up, the permeability of the fault gouge will decrease slowing as shown by the thick-upper line, whereas the permeability of the cataclasites may decrease initially during elastic loading compaction (thick line starting from "cemented cataclasite" in Fig. 11). Since fault gouge is much
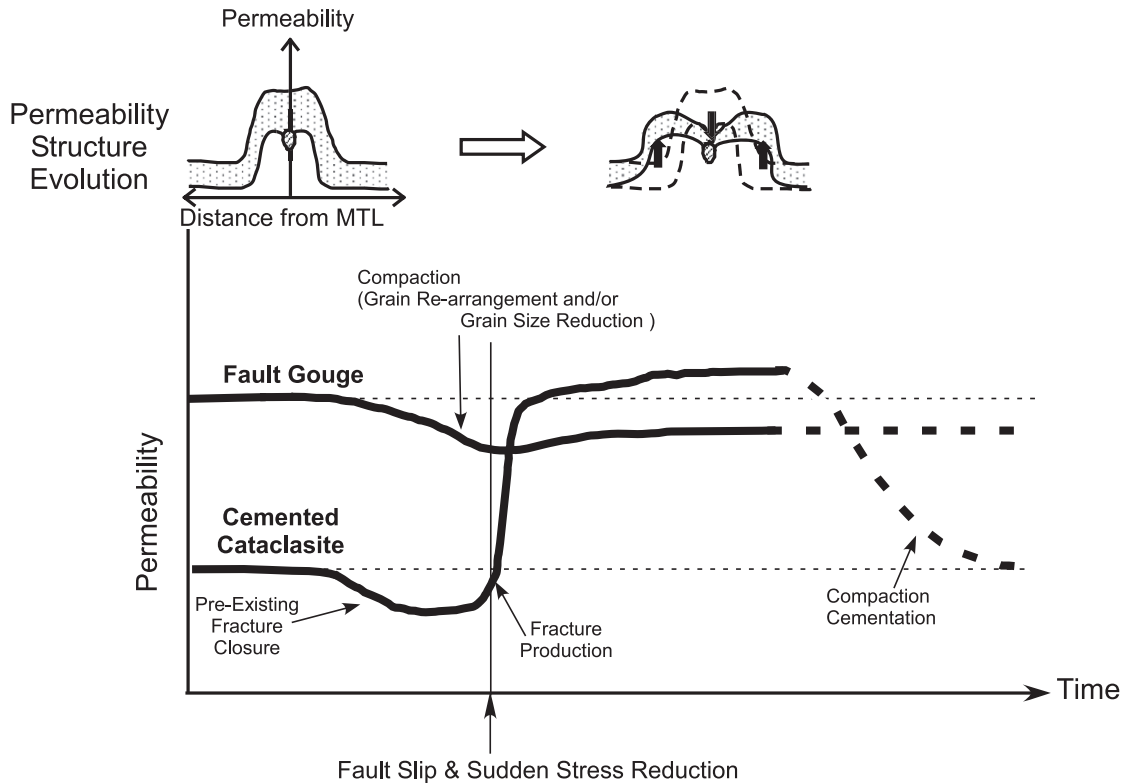
Fig. 11. A schematic diagram showing a possible model for the permeability evolution of fault gouge and cemented cataclasite during an earthquake cycle.

weaker than cataclasite (cf. Figs. 7 and 9; see also Fig. 10), it is unlikely that the cataclasite zone will suffer dilatancy prior to the earthquake although the cataclasite zone may fail very locally due to precursory slip. However, if the cataclasite zone fractures during and after a large earthquake, it may change into an even more permeable zone than the fault gouge zone (central part of Fig. 11). The permeability of fault gouge may increase somewhat owing to the release of stress (or reduction in the mean pressure), but a fractured cataclasite zone may become the most permeable portion in a fault zone during and after an earthquake. If fluid infiltration into the fractured cataclasite results in cementation, its permeability may decline slowing towards the next earthquake.

It must be kept in mind that stress changes during earthquakes are different from those in triaxial compression tests, so that our results can at best provide an insight into possible permeability evolution associated with a large earthquake. Full poroelastic and poro-

plastic parameters (e.g., Wang, 2000) need to be measured to address the permeability changes quantitatively due to general changes in stresses. Future studies must address the effects of large shearing deformation within fault zones, temperature and chemical cementation on the permeability using more examples of natural fault zones with variable lithology.

6. Conclusions

The Median Tectonic Line (MTL) at Ohshika, Central Japan, has a wide fault zone consisting of impermeable mylonite and cataclasite and fairly permeable incohesive fault rocks such as fault breccia and gouge. Cataclasite and fault gouge exhibit contrasting permeability changes with deformation. Permeability changes of cataclasite are similar to those for typical brittle rocks; the permeability reduces initially with nearly elastic compaction, turns to in-

crease with dilatant deformation prior to failure and shows abrupt increase upon cataclastic failure. On the other hand, permeability of fault gouge continues to decrease with deformation owing to continued compaction in triaxial compression. The permeability structure of a large-scale fault zone may change with time and the cataclasite zone may become a fluid conduit during and after a large earthquake. Full poroplastic parameters need to be measured for quantitative assessment of the changes in the permeability structure during earthquake cycles, including the effects of large inelastic deformation during an earthquake, temperature and long-term cementation.

Acknowledgements

References

Brace, W.F., Paulding Jr., B.W., Scholz, C., 1966. Dilatancy in the fracture of crystalline rocks. Journal of Geophysical Research 71, 3939–3953.

Caine, J.S., Evans, J.P., Forster, C.B., 1996. Fault zone architecture and permeability structure. Geology 24, 1025–1028.

Evans, J.P., Forster, C.B., Goddard, J.V., 1997. Permeability of fault-related rocks, and implications for hydraulic structure of fault zones. Journal of Structural Geology 19, 1393–1404.

Fischer, G.J., Paterson, M.S., 1992. Measurement of permeability and storage capacity in rocks during deformation at high temperature and pressure. In: Fault Mechanics and Transport Properties of Rocks. Academic Press, San Diego, CA, pp. 213–252.

Hara, I., Shyoji, K., Yokoyama, S., Arita, M., Hiraga, Y., 1977. Study on the southern marginal shear belt of the Ryoke metamorphic terrain—Initial movement picture of the Median Tectonic Line. Earth Science 31, 204–217 (in Japanese).

Hara, I., Shyoji, K., Sakurai, Y., Yokoyama, S., Hide, K., 1980. Origin of the Median Tectonic Line and its initial shape. Memoirs of the Geological Society 18, 27–49.

Kranz, R.L., Saltzman, J.S., Blacic, J.D., 1990. Hydraulic diffusivity measurements on laboratory rock samples using an oscillating pore pressure method. International Journal of Rock Mechanics and Mining Sciences & Geomechanics Abstracts 27, 345–352.

Lockner, D., Naka, H., Tanaka, H., Ikeda, R., 2000. Permeability and strength of core samples from the Nojima fault of the 1995 Kobe earthquake. Proceedings of the International Workshop on the Nojima Fault Core and Porehoke Data Analysis, pp. 147–152. US Geological Survey open-file report 00-129, GSJ interim report no. EQ/00/1.

Matsushima, N., 1994. A new interpretation of Median Tectonic Line of the Akaishi Mountain Lands, Japan. Bulletin of Iida city museum 4, 113–124 (in Japanese).

Michibayashi, K., 1993. Syntectonic development of a strain-independent steady state grain size during mylonitization. Tectonophysics 222, 151–164.

Michibayashi, K., Masuda, T., 1993. Shearing during progressive retrogression in granitoids: abrupt grain size reduction of quartz at the plastic-brittle transition for feldspar. Journal of Structural Geology 15, 1427–1432.

Mogi, K., 1967. Effect of the intermediate principal stress on rock failure. Journal of Geophysical Research 72, 5117–5131.

Morrow, C.A., Shi, L.Q., Byerlee, J.D., 1984. Permeability of fault gouge under confining pressure and shear stress. Journal of Geophysical Research 89, 3193–3200.

Paterson, M.S., 1978. Experimental Rock Deformation—The Brittle Field. Springer-Verlag, Berlin. 254 pp.

Seront, B., Wong, T.-F., Caine, J.S., Forster, G.B., Bruhn, R.L., 1998. Laboratory characterization of hydromechanical properties of a seismogenic normal fault system. Journal of Structural Geology 20, 865–881.

Takagi, H., 1983. Cataclastic deformation on mylonitic rocks along the Median Tectonic Line–Example in Kami-Ina district, Nagano Prefecture. Academic Studies (Biology, Geology) Issued Annually by the School of Education, Waseda University, 32, 47–60 (in Japanese).

Takagi, H., 1984. Mylonitic rocks along the Median Tectonic Line in Takato-Ichinose area, Nagano Prefecture. Journal of the Geological Society of Japan 90, 81–100 (in Japanese).

Takagi, H., 1986. Implications of mylonitic microstructures for the geotectonic evolution of the Median Tectonic Line, central Japan. Journal of Structural Geology 8, 3–14.

Tanaka, H., Takagi, H., Inoue, M., 1996. Mode of cataclastic deformation and hydrothermal alteration of the fault rocks and history of fault activity along the Median Tectonic Line, central Japan. The Journal of the Tectonic Research Group of Japan 41, 31–44 (in Japanese).

Uehara, S., 2002. Permeability structure of the Median Tectonic Line in Oshika-mura, Nagano Prefecture, central Japan, PhD Thesis, Kyoto University. 99 pp.

Walsh, J.B., 1965. The effect of cracks on the compressibility of rock. Journal of Geophysical Research 70, 381–389.

Wang, H.F., 2000. Theory of Linear Poroelasticity with Applications to Geomechanics and Hydrogeology. Princeton University Press, Oxford. 287 pp.

Wibberley, C.A.J., Shimamoto, T., 2003. Internal structure and permeability of major strike-slip fault zones: the Median Tectonic Line in Mie Prefecture, Southwest Japan. Journal of Structural Geology 25, 59–78.

Zhang, S., Cox, S.F., 2000. Enhancement of fluid permeability during shear deformation of a synthetic mud. Journal of Structural Geology 22, 1385–1393.

Zhang, S., Tullis, T.E., 1998. The effect of fault slip on permeability and permeability anisotropy in quartz gouge. Tectonophysics 295, 41–52.

Zhu, W., Wong, T.-F., 1997. The transition from brittle faulting to cataclastic flow: permeability evolution. Journal of Geophysical Research 102, 3027–3041.

Zhu, W., Wong, T.-F., 1999. Network modeling of the evolution of permeability and dilatancy in compact rock. Journal of Geophysical Research 104, 2963–2971.

Zoback, M.D., Byerlee, J.D., 1975. The effect of microcrack dilatancy on the permeability of Westerly granite. Journal of Geophysical Research 80, 752–755.